NEW NON-ORTHOGONALITY TREATMENT FOR ATMOSPHERIC BOUNDARY LAYER FLOW SIMULATION ABOVE HIGHLY NON-UNIFORM TERRAINS

by

Nikola S. MIRKOV [*] ***and Žarko M. STEVANOVIĆ***

Laboratory for Thermal Engineering and Energy, Vinca Institute of Nuclear Sciences,
University of Belgrade, Belgrade, Serbia

Original scientific paper
DOI: 10.2298/TSCI151025197M

In this paper we validate an improved finite volume approximation of Reynolds averaged Navier-Stokes equations for simulation of wind flows in body-fitted grids generated by algebraic extrusion from digital terrain elevation data, proposed in Mirkov et. al. [1]. The approach is based on second-order accurate finite volume method with collocated variable arrangement and pressure-velocity coupling trough SIMPLE algorithm. The main objective is the attenuation of spurious pressure field oscillations in regions with discontinuity in grid line slopes, as encountered in grids representing highly non-uniform terrains. Moreover, the approach relaxes the need for grid generation based on elliptic partial differential equation or grid smoothing by applying fixed point iterations (i. e. Gauss-Seidel) to initial grid node positions resulting from algebraic grid generators. Drawbacks of previous approaches which ignored treatment of finite volume grid cell cases with intersection point offset in non-orthogonality corrections are removed. Application to real-life wind farm project at Dobric (Svrljig, Serbia) is used to assess the effectiveness of the method. The results validate the view in which accurate discretization of governing equations play more important role than the choice of turbulence modeling closures.

Keywords: *wind flow, finite-volume method, non-orthogonal grids, complex terrains*

Introduction

Recently there is a significant growth in wind farm capacity in hilly, complex or even mountain terrains. Recent predictions (EWEA) suggest that this trend will continue due to available wind power capacity in these regions [2]. Non-uniformity in terrain elevation gives raise to complex flow behavior, *e. g.* stagnation regions, recirculation zones and regions of speed-up and slow-down in air velocity. Such flow characteristics should be well predicted in the process of wind farm siting where farm layout and specific positions of wind turbines are decided, which decisively influences the annual energy production. Therefore, the study of atmospheric boundary layer (ABL) over complex hilly and mountain terrains is very important in wind-farm planning cycle.

By definition, the ABL is the lowest layer of Earth atmosphere, thickness of which varies from a few tens of meters, in conditions of stable atmosphere, to around two kilome-

* Corresponding author; e-mail: nmirkov@vinca.rs

ters, depending on the weather conditions. The ABL, and especially its lowest layer – the surface layer, are directly influenced by local orography and surface roughness. Under these conditions, predicting the wind potential for energy productions is very difficult. The output power from a wind-turbine is proportional to wind speed to the third power, eq. (1), so even small speed-ups, caused by the local orography, causes significant increase in power:

$$P = \frac{1}{2} C_p \frac{D^2 \pi}{4} U^3 \tag{1}$$

Development of precise models for estimation of wind potential in regions with complex terrain is connected with a series of difficulties such as precise terrain representation, non-stationary character of the air flow, quality of turbulence models, and scarce data for validation in the form of full scale atmospheric measurements. One important study was that of Askervein hill [3], which was used in several turbulence modeling validation studies [4-6]. Other examples include turbulence modeling validation studies [7-9] based on the Bolund hill measurements [10].

Different level of errors produced in studies that used the same turbulence models brings to attention other sources of errors, most notable being discretization errors. This type of errors arise in second order finite volume simulations because of numerical approximation of integrals by mid-point rule. On non-orthogonal grids these errors are additionally amplified because of errors in interpolations, leading to decrease in the order of accuracy of the procedure. Modern computational fluid dynamics (CFD) codes [11, 12] include various corrections that remedy grid non-orthogonality, in which cell skewness is almost exclusively considered. In contrast to this practice, the algorithm validated in this study, consistently introduces corrections which treat situations that usually arise in grids generated over complex terrains, in which both cell skewness and so called *intersection-point offset* (explained in *Numerical algorithm*) appear.

In the present study we compare the proposed algorithm on a real test case of wind flow near Dobric, eastern Serbia. The test case considers potential wind farm location for which the meteorological measurement campaign was conducted by the authors during the period of 2010-2014. The test case also includes detailed information regarding topography and surface roughness. The purpose of the present study is both to validate the present algorithm using full scale atmospheric measurements and to compare its results with numerical results with other, widely available, commercial code for wind engineering applications. The results are intended to point out that the errors caused by different approximation practices in finite volume code, often play more dominant role than turbulence modeling errors.

Mathematical model

We are using Reynolds averaged Navier-Stokes equations as a model for turbulent flow of viscous incompressible flow:

$$\frac{\partial U_j}{\partial x_j} = 0 \tag{2}$$

$$\rho \frac{\partial U_i}{\partial t} + \rho U_j \frac{\partial U_i}{\partial x_j} = \frac{-\partial p}{\partial x_i} + \frac{\partial}{\partial x_j}\left[(\mu + \mu_t)\left(\frac{\partial U_i}{\partial x_j} + \frac{\partial U_j}{\partial x_i} \right) \right] \tag{3}$$

with additional initial and boundary conditions, where U_i is the mean velocity vector, p – the pressure, ρ – the density, μ – the molecular viscosity, μ_t – the eddy viscosity, x_i – the spatial Cartesian co-ordinate, and $i, j = 1, 2, 3$ are Cartesian component indices.

The two-equation k-ε turbulence model solves two additional transport equations for turbulence kinetic energy k and turbulence kinetic energy dissipation rate ε. These transport equations take the following forms, respectively:

$$\frac{\partial}{\partial t}(\rho k) + \frac{\partial(\rho k U_j)}{\partial x_j} = \frac{\partial}{\partial x_j}\left[\left(\mu + \frac{\mu_t}{\sigma_k}\right)\frac{\partial k}{\partial x_j}\right] + P_k - \rho\varepsilon \tag{4}$$

$$\frac{\partial}{\partial t}(\rho\varepsilon) + \frac{\partial(\rho\varepsilon U_j)}{\partial x_j} = \frac{\partial}{\partial x_j}\left[\left(\mu + \frac{\mu_t}{\sigma_\varepsilon}\right)\frac{\partial \varepsilon}{\partial x_j}\right] + \rho C_{\varepsilon 1} P_k \frac{\varepsilon}{k} - \rho C_{\varepsilon 2}\frac{\varepsilon^2}{k} \tag{5}$$

Production of turbulent kinetic energy trough mean velocity gradients P_k, is treated in following way:

$$P_k = -\rho\overline{u_i u_j}\frac{\partial U_i}{\partial x_j} = \mu_t\left(\frac{\partial U_i}{\partial x_j} + \frac{\partial U_j}{\partial x_i}\right)\frac{\partial U_i}{\partial x_j} = 2\mu_t S_{ij} S_{ij} = \mu_t |S|^2 \tag{6}$$

For the k-ε model, the eddy viscosity is calculated:

$$\mu_t = \rho C_\mu \frac{k^2}{\varepsilon} \tag{7}$$

Another variant different from standard k-ε model is its modification in which the coefficients are adjusted for ABL flow [4]. The coefficients of standard and modified k-ε turbulence model are listed in tab. 1.

Table 1. Coefficients for the standard k-ε turbulence model and k-ε turbulence model modified for atmospheric flows

	C_u	$C_{\varepsilon 1}$	$C_{\varepsilon 2}$	σ_k	σ_ε
Standard k-ε	0.09	1.44	1.92	1.0	1.3
Modified k-ε [4]	0.033	1.44	1.92	1.0	1.85

Simulation results using present procedure are compared with those obtained using WindSim software [13]. WindSim is an established tool often used in wind engineering community for wind farm siting applications. WindSim uses PHOENICS CFD code as its computational engine and simulations in this work used MIGAL coupled solver as an option implemented in PHOENICS [14, 15]. The MIGAL solves pressure and velocity fields simultaneously unlike segregated solvers based on SIMPLE algorithm. Besides Standard k-ε turbulence model, and its modification adjusted for flows in atmospheric boundary layer, simulation using WindSim software also included the RNG k-ε model [16] and Wilcox k-ω model [17] which are widely documented in the literature and in software documentation.

Numerical algorithm

The code used in the present study is based on the second-order finite volume method. The variable arrangement is cell-centered, pressure and velocities are collocated, and it is especially adapted for grids consisting of highly distorted computational cells [1]. The distinguishing characteristic of the present algorithm is consistent application of corrections taking

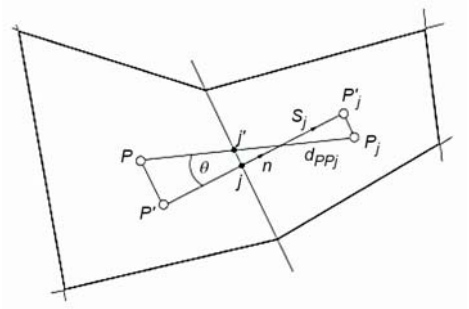

Figure 1. Typical cell arrangement in a non-orthogonal grid and important geometrical quantities. Non-orthogonality is defined by angle θ, and intersection point offset $\overline{jj'}$

into account the intersection-point offset in non-orthogonal grids. The offset is determined by distance between two points on cell face, one found at the intersection of line connecting two cell centers and the cell face, *j′*, and the cell face center *j*, fig. 1. This type of correction is, as shown previously in [1] crucial for higher accuracy of solution.

Accuracy of the calculation procedure strongly depends on the reconstruction of cell-centered gradients. In the present algorithm, a highly accurate least-squares gradient reconstruction procedure is used. It is based on the QR decomposition and devised to minimize the number of arithmetic operations needed in gradient field update, repeated several times during simulation, for all variables (pressure, velocity components, and turbulence scalars). Details of the procedure may be found in [1].

Convection term discretization is defined using the mid-point rule for approximation of the convection terms in integral form which lead to two unknowns, cell-face mass flux and cell-face interpolated value of dependent variable. The iterative process which follows the decoupling of pressure and velocity fields in SIMPLE algorithm [18, 19], allows the use of mass flux from the previous iteration, which introduces error due to lagging of mass flux value, which vanishes once the SIMPLE iterations converge. Mass fluxes on cell faces are calculated using the Rhie-Chow interpolation, usual for collocated cell arrangement [19, 20].

The cell-face interpolated value is found using the expression taking into account grid non-orthogonality and uses surrounding cell-center values of dependent variables, as well as their gradients, computed using the previously described least-squares procedure:

$$\overline{\phi_j} = \lambda_j \phi_P + (1-\lambda_j)\phi_{P_j} + \overline{\nabla\phi}\, d_{jj'}, \tag{8}$$

where $\lambda_j = d_j p_j / d_p p_j$ is the face interpolation factor. This leads to central differencing scheme corrected for non-orthogonality. Other options include flux-limited interpolation, adapted for non-orthogonal grids, which is described in detail in [1]. There is a variety of implemented flux-limiter schemes, such as MUSCL, SMART, and UMIST [21].

The second order approximation of the diffusion term using the mid-point rule leads to cell-face value of the gradient of dependent variable. The approximation of diffusion term therefore relies on accurate approximation of this quantity. The cell-face centered gradient is found by interpolation from the neighboring cell-centers in an original form which takes into account the gridnon-orthogonality. The procedure, defined as *power of cosθ relaxation approach*, is described in detail in [1]. It is a generalization of approaches including minimal correction approach and over-relaxed approach, which controls the effect on explicitly treated non-orthogonal correction to iterative process by a parameter depending on the angle θ (fig. 1), but in contrast to previous approaches takes into account the intersection-point offset [1].

The volumetric source terms are approximated using the mid-point rule.

The pressure and velocity fields are updated in a segregated manner within the SIMPLE iterative algorithm. The distinctive characteristic of the present algorithm is multiple pressure-correction solution to attenuate adverse effects of non-orthogonality to solution pro-

cedure. In additional pressure correction solutions, interpolations are conducted using the least-square gradients, not sensitive to loss of accuracy due to grid distortions [1].

In the present study we will exclusively use structured grids representing complex hilly terrain. When governing equations are discretized using the finite volume method on 3-D structured grids, the result is a linear system with well-defined sparsity pattern. Namely, the system matrix has diagonal structure, and number of diagonals is seven. For such linear systems, special iterative solution procedures have been devised, one popular choice being the session initiation protocol algorithm (SIP) [22]. One, more advanced, option uses SIP not as a standalone solver, but as the preconditioner for iterative solvers from the Krylov subspace family. Representative solvers of this type are PCG(SIP) and BiCGStab(SIP), which are used in the present algorithm [1].

For the flow over complex terrains, important type of boundary conditions is a rough wall boundary condition for velocity. For rough wall we use boundary-condition based on law-of-the-wall:

$$\frac{U}{u_\tau} = \frac{1}{\kappa} \ln\left[\min\left(E, \frac{E_{\mathrm{R}}}{E_{st}} \right) z_{pl} \right] \tag{9}$$

where von-Karman constant $\kappa = 0.41$, constant $E = 8.432$, and non-dimensional distance from wall $z_{pl} = zu_\tau/\nu$, $E_{st} = C_\mu^{1/4} k^{1/2} z_0/\mu$, $C_\mu = 0.09$, $E_{\mathrm{R}} = 30$, and z_0 is the surface roughness.

The present algorithm is implemented in an in-house code referred to as *Cappuccino*[*].

Dobric wind farm test case

Dobric, located in Svrljig municipality, eastern Serbia, is a potential wind farm location for which a four year measuring campaign has been carried out, during which the climatological data was gathered in order to assess wind potential for energy production. During the process various wind characteristics were estimated (*e. g.* field of wind speed-up, extreme fifty-year wind-U50, annual energy production for a given type of wind turbines, *etc.*) [23]. For that purpose various software tools were used. In particular WindSim CFD tool was used for the purpose of wind field prediction and wind potential for energy production estimate.

Based on these measurements, the wind climatology at Dobric is presented as a wind rose, showing the average wind speed distribution divided in velocity intervals (bins) and wind directions (sectors). The incoming wind directions are divided in 12 sectors, where the first sector is centered around north in fig. 2. The frequency table has been fitted to a Weibull distribution. Table 2 gives the Weibull shape and scale parameters (*k, A*), accumulated frequency of occurrence and the average wind speed for each sector, respectively.

Table 2. Weibull (*k, A*), frequency (% related to all sectors) and average wind speed [ms^{-1}] *vs.* sector (*H* = 50 m)

Sector	000	030	060	**090**	120	150	180	210	240	270	300	330
k	2.60	2.93	2.45	**2.40**	1.92	1.56	1.82	1.91	2.63	2.07	1.82	2.74
A	4.22	4.79	4.94	**6.30**	6.96	5.96	5.23	5.16	4.75	4.90	4.38	4.46
freq.	4.3	3.6	6.4	**25.6**	6.2	1.0	2.1	5.1	19.5	13.0	5.0	8.3
U	3.93	4.36	4.53	**5.75**	6.34	5.75	4.95	4.82	4.36	4.57	4.24	4.12

* To note that it is computer aided fluid flow analysis (CAFFA) with some field operation and manipulation (FOAM)

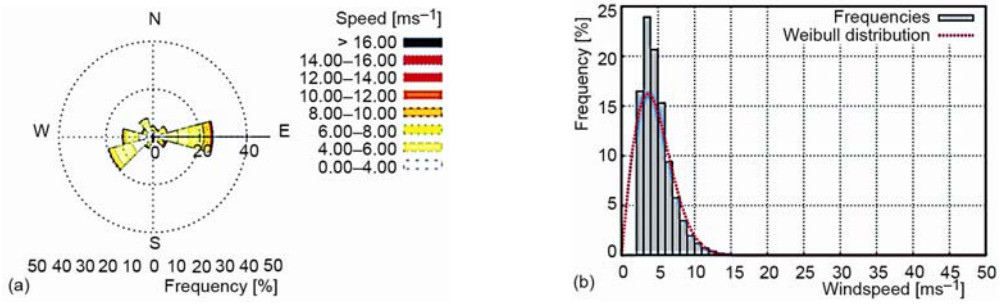

Figure 2. (a) Wind rose at Dobric measured at position x = 7604162.0, y = 4807154.0, at height above ground z_{gl} = 50.0 m. Mast position is determined in Transverse Mercator projection (Serbian-Hermann datum) – Zone 7, [24]; (b) frequency distribution fitted using Weibull distribution
(for color image see journal web-site)

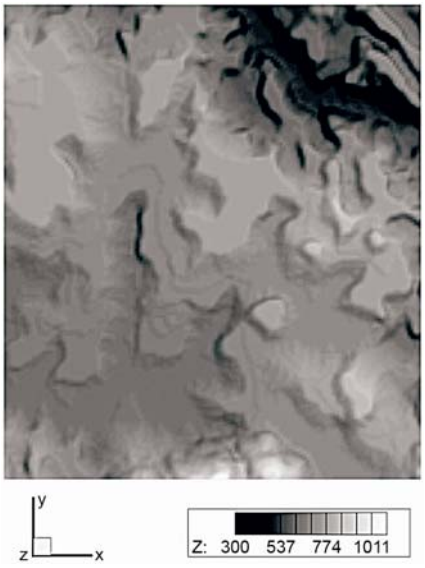

Figure 3. Terrain elevation map at Dobric. At south domain border are Svrljiske mountains

The data at the location of the measurement must, detailed map of terrain elevation and surface roughness, as well as the straightforward prescription of inlet conditions, provides enough input information for definition of the test case.

Details of numerical set-up

The terrain elevation map at Dobric is given in fig. 3. Digital terrain elevation and roughness data for Dobric test case is well defined and is provided at higher horizontal spatial resolution than one chosen for the present case. Because of very small variation, the terrain roughness is constant throughout the domain, and is set to the value z_0 = 0.03 m. This value is introduced in rough wall boundary condition for velocity.

Details of domain position, size, and horizontal spatial resolution are given in tab. 3. The grid extends 4654.0 m above the point in the terrain with the highest elevation. The grid is refined towards the ground. The vertical distribution of first ten cell centers is given in tab. 4, which is useful to estimate grid distribution near ground. Because of the terrain non-uniformity the grid point densities are different at places with different elevation. Table 4 therefore, shows vertical distributions at places of maximal and minimal elevation, respectively.

Table 3. Position, size and horizontal spatial resolution of computational domain

–	x-min	x-max	y-min	y-max	x-extent	y-extent	Resolution
[m]	7599000.0	7613000.0	4802000.0	4818000.0	14000.0	16000.0	100.0

Wind rose measured must give precise information on frequency and wind speed from different directions. Based on the wind rose, fig. 2(a), and table describing parameters related to

Table 4. Distribution of the first ten cell centers in vertical z-direction, relative to the ground, at the position with maximum and minimum elevation

Cell center no.	1	2	3	4	5	6	7	8	9	10
z-dist. max [m]	5.7	28.7	75.0	144.6	237.5	353.7	493.2	656.0	842.1	1051.5
z-dist. min [m]	6.6	33.5	87.7	169.1	277.8	413.7	576.9	767.3	985.0	1230.0

Weibull fitted distribution for over twelve sectors, tab. 2, we have chosen a single wind direction of 90° for present study. It is one of the most frequent and distinguished winds at the location, and is also convenient because of the computational cell alignment with flow direction.

It is important to point out here that further validation using flow directions which are not aligned with the direction of cells in structured mesh is necessary, because such conditions give rise to adverse effects, such as numerical diffusion, where proper discretization of convection terms (cf. flux limiter, Sweby diagram) is crucial.

Velocity and turbulence kinetic energy profiles are specified analytically along inflow borders. The analytical wind profiles are empirical profiles over flat terrain. The vertical profiles are dependent on the roughness height and on the stability of the atmosphere. Same applies for the turbulence profiles. In case of a neutral atmosphere the wind profiles follow logarithmic law. Applying the logarithmic profile along the border is equivalent to the placement of an infinite flat terrain upstream of the model. This may not be a correct assumption, but it will be good enough for the present study since it will be applied on both simulation codes in an identical way.

Depending on the given value for the Monin-Obukhov length the vertical profiles at the inlet are calculated. The linear temperature gradient over the whole atmosphere is assumed. Values of the stability parameter are taken in the range of –10000 to 10000 except 0. Default value of 10000 m (neutral atmosphere) is considered here.

The wind profiles in the higher elevations may differ considerably when stability of the atmosphere is taken into account. Therefore, a more convenient choice is to prescribe a reference speed in a reference height. In our case the reference speed is REFS = 8.2 m/s, and reference height of boundary layer is h_{BL} = 500 m. Using these input values, we define inlet profiles:

$$U = \frac{u_\tau}{\kappa} \ln\left(\frac{z - z_{\mathrm{gl}}}{z_0}\right) \qquad \text{if} \qquad (z - z_{\mathrm{gl}}) < h_{\mathrm{BL}} \tag{10}$$

$$U = U_{\mathrm{ref}} \qquad \text{if} \qquad (z - z_{\mathrm{gl}}) \geq h_{\mathrm{BL}} \tag{11}$$

where u_τ is the friction velocity devised from analytical relations (u_τ = 0.345843 m/s for present case), von-Karman's constant κ = 0.41, z_0 – the roughness, prescribed at constant value z_0 = 0.03 m based on terrain data file, and $(z - z_{\mathrm{gl}})$ – the height above ground level. For turbulence kinetic energy, the following relations are used:

$$k = \frac{{u_*}^2}{\sqrt{C_\mu}} \left(1 - \frac{z - z_{\mathrm{gl}}}{h_{\mathrm{BL}}}\right)^2 \qquad \text{if} \qquad (z - z_{\mathrm{gl}}) < h_{\mathrm{BL}} \tag{12}$$

$$k = 0 \qquad \text{if} \qquad (z - z_{\mathrm{gl}}) < h_{\mathrm{BL}} \tag{13}$$

Results

For the purpose of wind-farm siting, one of the important measures is wind speed-up by the terrain. For that purpose fig. 4 shows velocity magnitude at specified height above ground, z_{gl} = 10 m. The picture clearly shows regions of wind speed-up, which could be chosen as positions for wind turbines. Additionally, the velocity vectors in the same section are shown, necessary for decision of wind turbine orientation.

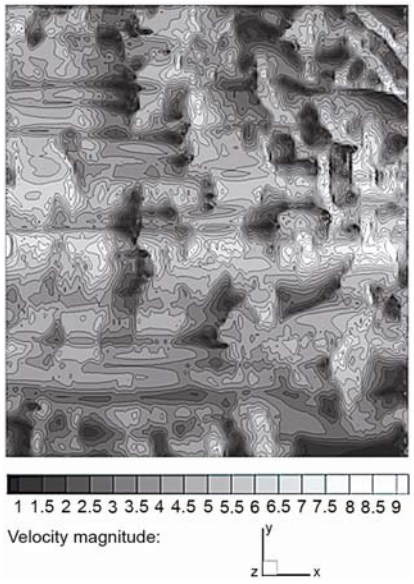

Figure 4. Velocity magnitude field and velocity vectors at fixed distance from gound z_{gl} = 10 m

The wind flow in this case (90° direction) goes along the mountain range known as the *Svrljiske planine*, which are seen on the southern edge of the domain. The effect of this mountain range on flow picture for present wind direction is seen in a slice shown in fig. 5(a). A unique location where vertical wind profiles are measured is meteorological mast located at x = 5162.0 m, y = 5154.0 m, in local coordinates. At this mast, anemometer probes are used to measure 10 minute averaged values of velocity and turbulence at three heights above ground, 10, 30, and 50 meters.

To assess the predictive capabilities of two CFD codes used, a diagram showing vertical profiles of velocity magnitude are shown in fig. 5(b). The results obtained using the WindSim include four different models. The present procedure shows profiles of Standard k-ε model and k-ε model with modifications for atmospheric boundary layer flows. We can see that the results obtained using the WindSim have very small mutual difference in predicted velocity profiles. In the diagram the profiles obtained by the present procedure show much better agreement with measured values compared to those obtained by WindSim. Complementing that, the tabs. 5 and 6 show velocity magnitudes and relative errors in computed results for present code and WindSim at three heights, corresponding to height of anemometer

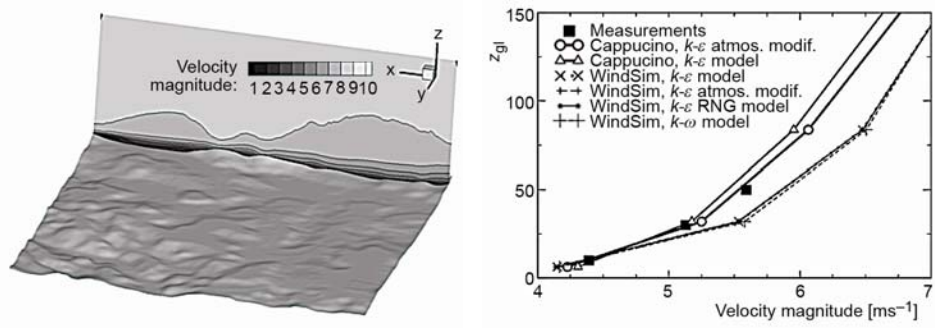

Figure 5. (a) Vertical cross-section in the flow direction along the slopes of Svrljiske mountain range, (b) Vertical profiles of velocity magnitude at position of the mast (located at x = 5162.0 m, y = 5154.0 m) obtained by WindSim and present algorithm (*Cappuccino*)

Table 5. Velocity magnitude (*relative error*) [%] pairs, calculated at various heights above ground at position of the meteorological must using WindSim

Height (z_{gl})	Measured	Standard k-ε	Modified k-ε	RNG k-ε	Wilcox k-ω
10 m	4.39	4.348 (*0.96*)	4.350 (*0.9*)	4.337 (*1.22*)	4.368 (*0.51*)
30 m	5.13	5.426 (*-5.77*)	5.427 (*-5.79*)	5.419 (*-5.64*)	5.469 (*-6.61*)
50 m	5.59	5.863 (*-4.88*)	5.863 (*-4.88*)	5.860 (*-4.82*)	5.901 (*-5.57*)

probes on meteorological mast. The plot and tables corroborate earlier observation that differences in prediction occur more often between same models implemented in two different codes than between two different turbulence models implemented. In present case, the reason can be traced to accuracy in numerical discretization and influence of discretization error to overall error, which often, in turbulence modeling validation studies, do not receive proper attention. This is particularly important in the case of wind flow over complex terrain simulations.

Table 6. Velocity magnitude (*relative error*) [%] pairs, calculated at various heights above ground at position of the meteorological must using the present procedure

Height (z_{gl})	Measured	Standard k-ε	Modified k-ε
10 m	4.39	4.431 (*0.009*)	4.374 (*-0.004*)
30 m	5.13	5.108 (*-0.004*)	5.170 (*0.008*)
50 m	5.59	5.446 (*-0.026*)	5.533 (*-0.010*)

Tables 7 and 8 show turbulence intensity calculated by present algorithm and WindSim at various heights above ground level at position of the measuring mast. The turbulence intensity is calculated using following expression:

$$Ti = 100 \frac{\sqrt{4/3k}}{\sqrt{U^2 + V^2 + W^2}} \ [\%] \tag{14}$$

whrere U, V, and W are Cartesian components of mean velocity.

Table 7. Turbulence intensity (*relative error*) [%] pairs, calculated at various heights above ground at position of the meteorological must, using WindSim

Height (z_{gl})	Measured	Standard k-ε	Modified k-ε	RNG k-ε	Wilcox k-ω
10 m	17.54	16.082 (*-8.31*)	16.087 (*-8.28*)	16.289 (*-7.13*)	16.122 (*-8.08*)
30 m	14.62	14.989 (*2.52*)	15.024 (*2.77*)	14.900 (*1.92*)	15.209 (*4.03*)
50 m	13.42	13.420 (*0.02*)	13.455 (*0.29*)	13.343 (*-0.55*)	13.803 (*2.88*)

Conclusions

In this paper we presented a comparative assessment of two CFD codes for simulation of flow in the atmospheric boundary layer over real, highly complex terrain. The codes were used on a real test case of Dobric wind farm, for which a well-defined

Table 8. Turbulence intensity (*relative error*) [%] pairs, calculated at various heights above ground at position of the meteorological mast, using the present procedure

Height (z_{gl})	Measured	Standard k-ε	Modified k-ε
10 m	17.54	10.852 (*-38.13*)	11.298 (*-35.59*)
30 m	14.62	11.628 (*-20.46*)	12.273 (*-16.05*)
50 m	13.42	10.024 (*-25.31*)	10.152 (*-24.35*)

geometry and full atmospheric scale measurements are available. It is demonstrated that differences in numerical discretization result in greater differences than those between various turbulence models implemented in the same code. It is shown that the present algorithm, which included more elaborate corrections for highly non-orthogonal grids which result in wind flow over complex terrain application, gives more precise results, when same turbulence closures were employed in both cases. The additional computational cost caused by the introduced non-orthogonal corrections used by the present algorithm is negligible.

Acknowledgments

This work was supported by the Ministry of Education, Science and Technological Development of the Republic of Serbia (grant TR-33036).

Nomenclature

C_p – drag coefficient, [–]
D – diameter of wind turbine, [m]
E – law of the wall constant, [–]
E_R – rough wall b. c. constant, [–]
h_{BL} – boundary layer height, [m]
k – turbulence kinetic energy, [$m^{-2}s^{-2}$]
P – power, [W]
REFS – referent speed above h_{BL}, [ms^{-1}]
t – time, [s]
U – average wind spead, [ms^{-1}]
u – shear velocity, [ms^{-1}]
u_τ – friction velocity, [ms^{-1}]
z^+ – non-dimenzional distance to wall, [–]
z_0 – surface roughness, [m]
z_{gl} – height above ground level, [m]

Greek symbols

ε – turbulence kinetic energy dissipation rate, [$m^{-2}s^{-3}$]
κ – von Karman's constant, [–]
λ_j – linear interpolation factor for cell face j, [–]
μ – molecular viscosity, [Pa·s]
μ_t – eddy viscosity, [Pa·s]
ρ – fluid density, [kgm^{-3}]
σ_k – turbulent Prandtl number, [–]
φ – dependent variable, [–]
ω – specific turbulence dissipation rate, mean turbulence frequency, [$1s^{-1}$]

Subscripts

P, P_j – value pertinent to current or neighboring cell center respectively
i, j – Cartesian component indices

References

[1] Mirkov, N., *et al.*, On the Improved Finite Volume Procedure for Simulation of Turbulent Flows over Real Complex Terrains, *Journal of Computational Physics*, *287* (2015), Apr., pp. 18-45
[2] ***, Wind Energy Scenarios for 2020, http://www.ewea.org.
[3] Taylor, P. A., Teunissen H. W., The Askervein Hill Project: Report on September/October 1983 Main Field Experiment, Rep. MSRB-84-6. Technical report, Atmospheric Environment Service, North York, Ont., Canada, 1985
[4] Beljaars, A. C. M., *et al.*, A Mixed Spectral Finite-Difference Model for Neutrally Stratified Boundary-Layer Flow over Roughness Changes and Topography, *Boundary Layer Meteorology*, *38* (1987), 3, pp. 273-303
[5] Undheim, O., *et al.*, Nonlinear, Microscale Modelling of the Flow over a Skervein Hill, *Boundary Layer Meteorology*, *120* (2006), 3, pp. 477-495
[6] Stevanović, Ž., *et al.*, Validation of Atmospheric Boundary Layer Turbulence Model by On-Site Measurements, *Thermal Science, 14* (2010), 1, pp. 199-207
[7] Bechmann, A., *et al.*, The Bolund Experiment, Part II: Blind Comparison of Microscale Flow Models, *Boundary-Layer Meteorology*, *141* (2011), 2, pp. 245-271
[8] Prospathopoulos, J. M., *et al.*, Application of a 3D RANS Solver on the Complex Hill of Bolund and Assessment of the Wind Flow Predictions, *Journal of Wind Engineering and Industrial Aerodynamics*, *107-108 (*2012), Aug., pp. 149-159
[9] Vuorinen, V., *et al.*, Large-Eddy Simulation in a Complex Hill Terrain Enabled by a Compact Fractional Step Open Foam Solver, *Advances in Engineering Software*, *79* (2015), C, pp. 70-80

[10] Berg, J., *et al.*, The Bolund Experiment, Part I: Flow over a Steep, Three-Dimensional Hill, *Boundary Layer Meteorology*, *141* (2011), 2, pp. 219-243
[11] Mathur, S. R., Murthy, J. Y., A Pressure-Based Method for Unstructured Meshes, *Numerical Heat Transfer, Part B: Fundamentals*, *31* (1997), 2, pp. 195-215
[12] Jasak, H., *et al.*, High Resolution NVD Differencing Scheme for Arbitrarily Unstructured Meshes, *International Journal for Numerical Methods in Fluids*, *31* (1999), 2, pp. 431-449
[13] ***, WindSim, User Documentation (www.windsim.com)
[14] ***, Phoenics Documentation, CHAM Ltd. (www.cham.co.uk)
[15] Ferry, M., New Features of MIGAL Solver, *Proceedings*, 9th Phoenics User Conference, Moscow, 2002
[16] Yakhot, V., *et al.*, Development of Turbulence Models for Shear Flows by a Double Expansion Technique, *Physics of Fluids A*, *4* (1992), 7, pp. 1510-1520
[17] Wilcox, D., *Turbulence Modeling for CFD,* 2nd ed., DCW Industries, La Canada, Flintridge, Cal., USA, 1998
[18] Patankar, S. V., *Numerical Heat Transfer and Fluid Flow*, McGraw-Hill, New York, USA, 1980
[19] Rhie, C. M., Chow, W. L., Numerical Study of the Turbulent Flow Past an Airfoil with Trailing Edge Separation, *AIAA Journal*, *21* (1983), 11, pp. 1525-1532
[20] Ferziger, J. H., Perić, M., *Computational Methods for Fluid Dynamics*, 2nd ed., Springer, Berlin, 1999
[21] Waterson, N. P., Deconinck, H., Design Principles for Bounded Higher-Order Convection Schemes – a Unified Approach, *Journal of Computational Physics*, *224* (2007), 1, pp. 182-207
[22] Stone, H., Iterative Solution of Implicit Approximations of Multi-Dimensional Partial Differential Equations, *SIAM Journal on Numerical Analysis*, *5* (1968), 3, pp. 530-568
[23] Stefanović, Ž., *et al.*, Referent Wind Speed and Turbulence Intensity Estimation and On-Site Wind Turbines Classification, *Proceedings*, 16th Symposium on Thermal Science and Engineering of Serbia, Sokobanja, Serbia, 2013
[24] ***, http://pedja.supurovic.net/veza/312

Paper submitted: October 25, 2015
Paper revised: November 4, 2015
Paper accepted: November 5, 2015